RSC Advances

ROYAL SOCIETY OF CHEMISTRY

www.rsc.org/advances

• Effects of nitrogen-dopants on Ru-supported catalysts for acetylene hydrochlorination

Lijun Hou,[a] Jinli Zhang,[a] Yanfeng Pu*[b] and Wei Li*[a]

[a] School of Chemical Engineering and Technology, Tianjin University, Tianjin 300072, P. R. China. E-mail: liwei@tju.edu.cn

[b] State Key Laboratory of Coal Conversation, Institute of Coal Chemistry, Chinese Academy of Sciences, Taiyuan 030001, P. R. China. E-mail: puyanfeng@sxicc.ac.cn

Abstract

A series of N-doped spherical active carbon were synthesized via the pyrolysis of melamine in activated carbon, and used as the support to prepare Ru-based catalysts for acetylene hydrochlorination reaction. The catalytic performance assessments indicate that the N-doped carbon support can increase greatly the activity and the stability of Ru-based catalysts. The optimal activity is achieved over Ru/SAC-N700, with the acetylene conversion of 99.8% under the conditions of 170 °C, C_2H_2 gas hour space velocity (GHSV) of 180 h^{-1}, the feed volume ratio of V(HCl)/V(C_2H_2) of 1.1 after 30 h. Using characterizations of BET, FT-IR, XPS, TPR, TPD, TG, etc., it is illustrated that N-dopants can increase the dispersion of Ru elements, enhance the adsorption of reactants and the desorption of the product, and reduce significantly the coke deposition, consequently resulting in higher catalytic activity of Ru/SAC-N700. It is suggested that the pyridine-nitrogen plays an important role in augment of catalytic activity of Ru-supported catalysts.

Keywords: acetylene hydrochlorination, N-doped carbon, Ru catalysts

1. Introduction

Acetylene hydrochlorination reaction is the dominant pathway to produce vinyl chloride monomer (VCM) in polyvinyl chloride (PVC) industry of China, which currently utilizes carbon-supported $HgCl_2$ as the catalyst. However, mercuric chloride is highly toxicity and tends to sublimate, resulting in the severe environmental pollution problems.[1] In 2013, more than 140 countries signed "the Minamata Convention on Mercury" so as to inhibit the trade and application of mercury over the world.[2] Hence, it is urgent to explore environmental-benigh non-mercury catalysts for acetylene

hydrochlorination.

Non-mercuric noble metallic catalysts, involving Au,[3-8] Pd,[9] Pt,[10, 11] etc., have been studied for the acetylene hydrochlorination, following the pioneer work of Hutchings[12] on Au catalysts. Taking into account the cost of the catalyst, the Ru-based catalyst is considered as a promising candidate for the non-mercury catalyst of acetylene hydrochlorination.[13-18] For instance, the bimetallic Ru1Co3/SAC catalyst showed an acetylene conversion of 95% after 48 h under the condition of 170 °C and C_2H_2 GHSV of 180 h^{-1}.[17] The Cu-Ru catalyst supported on carbon nanotubes (Cu400Ru/MWCNTs) showed an acetylene conversion of 51.6% at the conditions of 180 °C, V(HCl)/V(C_2H_2) = 1.2 and GHSV(C_2H_2) = 180 h^{-1}.[16] However, it is essential to improve further the catalytic activity for ruthenium-based catalysts, so as to develop an efficient non-mercury catalyst for acetylene hydrochlorination in the view of industrial application.

Heteroatom-doped carbon materials have shown promising properties to prepare electrodes in supercapacitors[19], electrocatalysts for the oxygen reduction reaction (ORR) in fuel cells.[20,21] and cathode materials for lithium ion batteries, [22, 23] etc. In particular, Bao and coworkers[24] prepared a nanocomposite of nitrogen-doped carbon, which showed catalytic activity for acetylene hydrochlorination, with the acetylene conversion of 80% at 200 °C and a space velocity of 30 h^{-1}. Dai et al. [25] prepared B, N-doped graphene catalysts, which showed the initial acetylene conversion about 95% under the conditions of 150 °C, C_2H_2 GHSV of 36 h^{-1}. Zhou et al.[26] reported a Cu-based catalyst supported N-doped carbon nanotubes, showing the initial acetylene conversion about 45.8% under the conditions of 180 °C and C_2H_2 GHSV of 180 h^{-1}. Recently, Zhao et al. reported that the N-doped carbon support can increase the activity of Ru-based catalysts for the

reaction of acetylene and 1, 2-dichloroethane (EDC) at 250 °C and total liquid hourly space velocity of EDC 0.2 h^{-1}.[27] Therefore, we are inspired to study the effect of N-doped carbon supports on the activity of Ru-based catalysts for acetylene hydrochlorination.

In this article, we prepared a serious of Ru-based catalysts with the support of N-doped spherical active carbon synthesized via the pyrolysis of melamine in activated carbon, and assessed the catalytic activity for acetylene hydrochlorination. The results show that with the N-doped carbon support, the activity and the stability of Ru-based catalysts are increased greatly. The influence of N-dopant on the structural, adsorption properties and active species of Ru-based catalysts were characterized by BET, FT-IR, XPS, TPR, TPD, TG, etc.

2. Experimental

2.1 Catalyst preparation

In a typical experiment, the pitch-based spherical activated carbon (SAC, 10 g, 20–40 mesh) was mixed with melamine (5 g) in deionized water (50 mL) at 343 K under stirring for 18 h. After filtration, the mixture was dried at 393 K overnight under vacuum, and then experienced the carbonization at the temperature of 600, 700 or 800 °C for 1 h in a quartz tube under N_2 atmosphere at a flow of 100 cm^3 min^{-1} with a heating rate of 10 K min^{-1}. The obtained N-doped carbon samples were denoted as SAC-N600, SAC-N700 and SAC-N800, respectively.

The Ru-based catalysts (Ru/SAC-N) were prepared via a wetness impregnation technique using the N-doped carbon as the support. A solution of $RuCl_3$ (209.5 mg) in deionized water (12 mL) was added dropwise to the N-doped carbon (10 g) under stirring at room temperature, followed by aging at 60 °C for 12 h. The product was then dried at

150 °C for 12 h and then assessed the catalytic performance for acetylene hydrochlorination. The obtained samples were denoted as Ru/SAC-N600, Ru/SAC-N700 and Ru/SAC-N800 with the support of SAC-N600, SAC-N700 and SAC-N800, respectively.

As a control, undoped activated carbon was also used as the support to prepare the Ru-based catalyst via the similar technique, and denoted as Ru/SAC.

2.2 Catalyst tests

Catalysts were assessed in a fixed-bed stainless steel micro-reactor (i.d. of 10 mm) for acetylene hydrochlorination. The temperature of the reactor was regulated by CKW-1100 temperature controller produced by Chaoyang automation instrument factory (Beijing, China). The pipeline was purged with nitrogen before the reaction to remove water and air in the system, then acetylene (15 mL min^{-1}) and hydrogen chloride (16.5 mL min^{-1}) were fed through filters to remove trace impurities and via calibrated mass flow controllers into the heated reactor containing the catalyst (5 mL), operated at 170 °C under the atmosphere pressure with a GHSV (C_2H_2) of 180 h^{-1}. The effluent from the reactor was passed through a 10% sodium hydroxide aqueous solution to absorb the unreacted hydrogen chloride, and then analyzed by gas chromatograph (GC-3420 by Beijing Beifen-Ruili Analytical Instrument Co. Ltd.), equipped with FID detector. The acetylene conversion (X_A) and the selectivity to VCM (S_{VC}) were calculated by the equations (1) and (2), respectively.

$$X_A = \frac{\emptyset_{A0} - \emptyset_A}{\emptyset_{A0}} \times 100\% \quad (1)$$

$$S_{VC} = \frac{\emptyset_{VC}}{(1-\emptyset_A)} \times 100\% \quad (2)$$

Where $\emptyset_{A0}$ = the volume fraction of acetylene in the feed and $\emptyset_A$ = the volume fraction of remaining acetylene in the effluent from the reactor, respectively. $\emptyset_{VC}$ is the volume fraction of vinyl chloride in the effluent from the reactor.

2.3. Catalyst characterization

The pore size distribution and specific surface areas of the catalysts were analyzed by ASAP 2020C surface area and porosity analyzer (Micromeritics Instrument Corporation, USA), degassing for 6 h at 423 K, then analyzed with liquid nitrogen adsorption at 77 K.

The Fourier transform infrared spectroscopy (FT-IR) was performed using a Bruker Vertex 70 FT-IR spectrophotometer equipped with a MCT detector at a resolution of 4 cm^{-1}.

Raman spectra were measured with Renishaw inVia reflex, with the resolution of 4 cm^{-1} (632.8 nm).

Thermogravimetric analysis (TGA) was carried out with TG-DTG simultaneous thermal analyzer (NETZSCH STA 449F3 Jupiter®, Germany) under nitrogen atmosphere at a flow rate of 100 mL min^{-1} with a heating rate of 10 °C min^{-1}.

X-ray photoelectron spectra (XPS) were recorded on a PHI-5000 Versa probe II-X System. The binding energy was calibrated with respect to the C 1s level 284.80 eV of aliphatic carbon.

Transmission electron microscopy (TEM) was conducted using a JEM2100F TEM and an FEI Titan 80-300 TEM/STEM, equipped with CEOS spherical aberration corrector. The samples were dispersed in ethanol and supported on carbon-film-coated copper grids before the characterization of TEM.

Temperature-programmed reduction (TPR) experiments were performed using AutoChem 2910 to determine the reduction behavior of the catalysts. For each experiment, the sample was heated from 35 °C to 800 °C with a heating rate of 10 °C min^{-1}. The flow gas mixture is 5% H_2/Ar with a flow rate of 20 mL/min.

Temperature programmed desorption (TPD) was measured by an AutoChem BET TPR/TPD (Quantachrome Instruments AMI-90). The weight of the each sample was fixed at 130 mg. For C_2H_2-TPD and HCl-TPD profiles, the samples were first pre-treated under C_2H_2 and HCl atmosphere respectively for 4 h at reaction temperature (170 °C), then pure helium was pass through the samples for 30 min and the desorption profiles were recorded from 50 °C to 700 °C at a heating rate of 10 °C min^{-1}. Similarly, the VCM-TPD profiles were recorded, except the pretreatment condition of VCM is at 100 °C for 1 h. For CO-TPD, the samples were first reduced at 400 °C for 2 h in 10% H_2/Ar followed by cooling to room temperature, and then 250 uL pulse of 10% CO/Ar were introduced, and the CO uptake profile was measured by a TCD detector.

3. Results and discussion

3.1 N-doped carbon supports

BET measurements were performed to investigate the physical structure variation of carbon resulted by N-doping. Table 1 lists the specific surface area, pore volume and average pore diameter of SAC, SAC-N600, SAC-N700 and SAC-N800. The N_2 adsorption-desorption isotherms (Fig. S1a) exhibit the type Ⅰ adsorption curves, corresponding to the microporous structure. The pore size distributions of N-doped carbon supports are centered at 5Å according to HK model (Fig. S1b), approximate to that of SAC. The N-doped carbon samples show higher surface area and total pore

volume that of SAC, and SAC-N700 exhibits the highest surface area (1325 $m^2 g^{-1}$) and total pore volume of 0.69 $cm^3 g^{-1}$. Previously, Wang et al.[28] adopted ammonia to treat mesoporous carbon in order to prepare the catalytic material for oxygen reduction reaction, and obtained N-doped carbon with increased surface area (2021 m^2/g), much higher than the undoped carbon (658 m^2/g). On the other hand, Saiter and coworkers[29] reported that ammonia could be generated during the decomposition of melamine at high temperature. Therefore, it is reasonable to consider that the intermediate of ammonia, decomposed from melamine, can etch the porous carbon so as to make the surface area and the pore volume of carbon increased.

Table 1 Pore structure parameters of the supports

Samples	S_{BET} ($m^2 g^{-1}$)	Pore volume ($cm^3 g^{-1}$)	Pore diameter (Å)
SAC	1066	0.62	5.02
SAC-N600	1144	0.63	4.82
SAC-N700	1325	0.69	4.84
SAC-N800	1237	0.64	4.80

FT-IR spectra were measured to characterize the surface functional groups of undoped and N-doped SAC. As shown in Fig. 1, SAC has major bands at 1625 cm^{-1} and 3423 cm^{-1}, which are respectively attributed to the C=C and O-H stretching vibrations, besides the bands at 1037 cm^{-1} and 1400 cm^{-1}, which are due to the stretching of C-O and the stretching vibration of the carboxyl groups.[30-32] For N-doped SAC, the intensities of bands at 1037 cm^{-1} and 3423 cm^{-1} are weaker than those of SAC. For SAC-N700 and SAC-N800, a small new band is observed at 1590 cm^{-1}, which is attributed to the stretching of C=N groups, [33, 34] together with another band at 3120 cm^{-1}, which is attributed to the N-H and/or NH_2 groups. [35-37] It is suggested that the structure of the N-doped SAC consists of more nitrogen-containing functional groups and less content of

159 oxygen functional groups, comparing with undoped SAC.

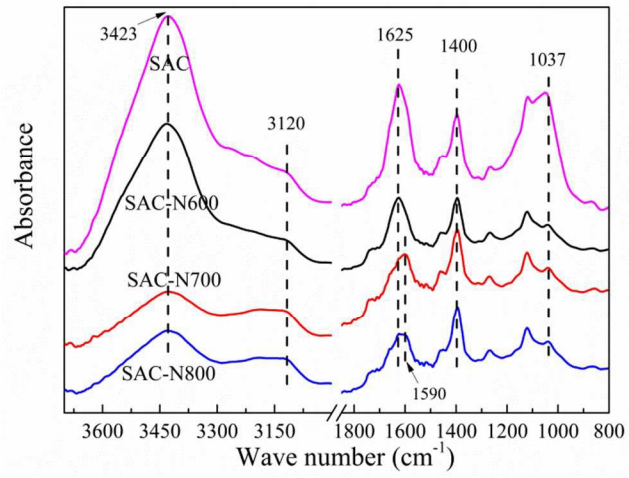

160

161 **Fig. 1** FT-IR spectra of different support samples.

162

163 **Table 2** Elemental compositions on the surface of the samples determined by XPS analysis

	Element composition (%)		
Samples	C	N	O
SAC	96.2	0	3.8
SAC-N600	96.0	1.4	2.6
SAC-N700	94.8	2.0	3.2
SAC-N800	94.9	1.8	3.3

164

165 **Table 3** Relative contents and binding energies of nitrogen species of the N-doped samples

	Area%, binding energy(eV)			
Samples	N_P	N_{PYR}	N_Q	N–X
SAC	-	-	-	-
SAC-N600	39.6 (398.2)	31.2 (400.0)	20.8 (401.4)	8.4 (402.7)
SAC-N700	56.9 (398.7)	8.8 (400.2)	30.9 (401.2)	3.4 (402.5)
SAC-N800	45.0 (398.4)	36.9 (400.0)	6.7 (401.4)	11.4 (402.4)

166

167 XPS spectra of different carbon samples were analyzed to distinguish the elemental
168 compositions and the species of nitrogen dopants, comparing with the undoped SAC
169 sample. As listed in Table 2, the elemental compositions of the undoped SAC sample are
170 96.2% carbon and 3.8% oxygen. While for the N-doped samples, there are nitrogen
171 component, the nitrogen content equals respectively 1.4% for SAC-N600, 2.0% for

SAC-N700 and 1.8% for SAC-N800. Fig. S2 displays the deconvolution of the N 1s XPS spectra, indicating the existence of four kinds of nitrogen species including the pyridine-nitrogen (N_P) near 398.4 eV, the pyrrole-nitrogen (N_{PYR}) at 400.1 eV, the quaternary-nitrogen (N_Q) at 401.3 and the nitrogen oxides (N–X) near 402.5 eV. Table 3 lists the content of each nitrogen species in the N-doped SAC. It is clear that the pyridine-nitrogen (N_P) is the dominant nitrogen species in SAC-N600, SAC-N700, and SAC-N800, while the N content is dependent on the calcination temperature. The SAC-N700 sample has the highest amount of pyridine-nitrogen (N_P, 56.9%) but the least amount of pyrrole-nitrogen (N_{PYR}, 8.8%).

Previously, Wong et al.[38] prepared the nitrogen-doped graphene (nG) via pyrolysis of graphene oxide at the temperature from 400 to 1000 °C using the nitrogen-precursor of melamine, and the obtained nG consisting of the quaternary N (5%), carbon nitride and oxygenated N. In addition, Xia et al.[39] suggested that melamine molecules adsorbed onto graphite oxide (GO) surfaces could be condensed into carbon nitride with increasing temperature, and the removal process of oxygen species at high temperature could provide active sites for nitrogen doping into graphene frameworks.

Saiter and coworkers[29] reported that ammonia could be generated during the decomposition of melamine at high temperature. The possible mechanism for doping N in carbon is associated with the oxygen-containing groups in the undoped SAC sample (Table 2). The intermediates decomposed from melamine, including ammonia, can react with the oxygen-containing groups in the SAC to make N dopants intercalated into the carbon materials. It deserves to study the mechanism for N-doping in this process in our future work. Table S2 lists the elemental composition of different SAC samples

determined by elemental analysis (Vario Micro, Elementar). It is indicated that the bulky element composition of carbon samples are approximate to those determined by XPS (Table 2). Therefore, the N dopants are located uniformly in the carbon supports, rather than on the surface.

3.2 N-doped carbon supported Ru catalysts

Fig. 2 displays the catalytic performance of the supported Ru catalysts and the individual supports. The SAC-N700 support shows the initial acetylene conversion of 39.0% and decreases to 32.0% in 30 h, much higher than those over the support SAC, suggesting that N-dopants can enhance the catalytic activity of the carbon support toward acetylene hydrochlorination. Over the Ru catalyst supported on SAC (Ru/SAC), the initial acetylene conversion is 89.4%, reducing to 85.2% in 30 h. While using the N-doped SAC as the support, the Ru catalysts display significant increase of catalytic activity. The initial acetylene conversion is 96.1% over Ru/SAC-N600, 99.5% over Ru/SAC-N700, and 98.5% over Ru/SAC-N800, respectively. In particular, after 30 h, the acetylene conversion over Ru/SAC-N700 is 99.8%, suggesting a superior catalytic stability. As for the selectivity to VCM, it is 99.5% over Ru/SAC, 99.8% over Ru/SAC-N600, 99.9% over Ru/SAC-N700 and 99.8% over Ru/SAC-N800, respectively. It is illustrated that N-doped SAC supports indeed improve the activity and stability of the Ru catalysts.

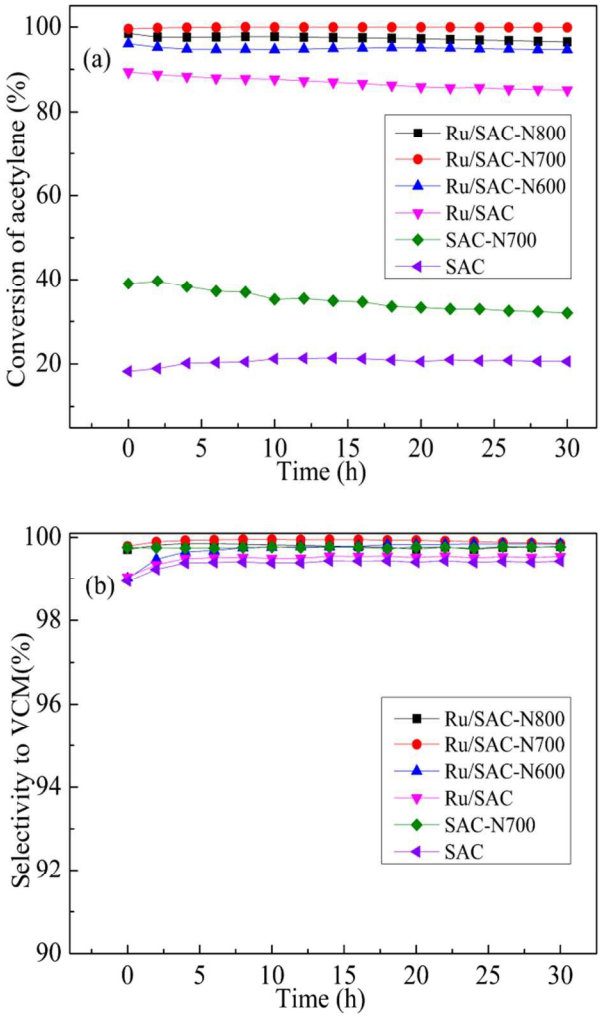

Fig. 2 The conversion of acetylene (a) and selectivity to VCM (b) over SAC, SAC-N700, Ru/SAC, Ru/SAC-N600, Ru/SAC-N700 and Ru/SAC-N800. Reaction conditions: T=170 °C, V(HCl)/V(C_2H_2)=1.1:1, GHSV(C_2H_2)=180 h^{-1}.

Table 4 lists the dispersion of Ru elements calculated on the basis of CO adsorption. The dispersion is 37.5% for the Ru/SAC. For the Ru/SAC-N catalysts, the Ru dispersion is higher, with the highest dispersion of 49.9% corresponding to the catalyst Ru/SAC-N700, followed by Ru/SAC-N800 (49.0%) and Ru/SAC-N600 (48.2%). The results illustrate that N-dopants can facilitate the dispersion of Ru nanoparticles, probably due to the more defect sites caused by N dopants, which can anchor stably the active Ru

224 species.

225 **Table 4** Ru dispersion calculated according to CO uptake

Samples	CO uptake (μmol CO/g)	Ru dispersion (%)
Ru/SAC	37.1	37.5
Ru/SAC-N600	47.7	48.2
Ru/SAC-N700	49.4	49.9
Ru/SAC-N800	48.5	49.0

226

227 Fig. 3 displays the TEM images of the fresh and used catalysts. There are some
228 small black dots in the image, which are highly dispersed Ru particles on the support.
229 The average size is about 1.40 nm and 1.24 nm for the fresh Ru/SAC and fresh
230 Ru/SAC-N700 catalysts, respectively. This result indicates that the N dopants improve
231 the Ru dispersion of catalysts, which is in accord with the CO-TPD results (Table 4).
232 While for the used Ru/SAC and used Ru/SAC-N700, obvious larger black dots appear in
233 the images, suggesting somewhat aggregation or coke deposition during the reaction. The
234 average particle size of the used Ru/SAC is 2.18 nm, much larger than that of the used
235 Ru/SAC-N700 (1.63 nm), indicating that N dopants can inhibit the aggregation or coke
236 deposition during the reaction.

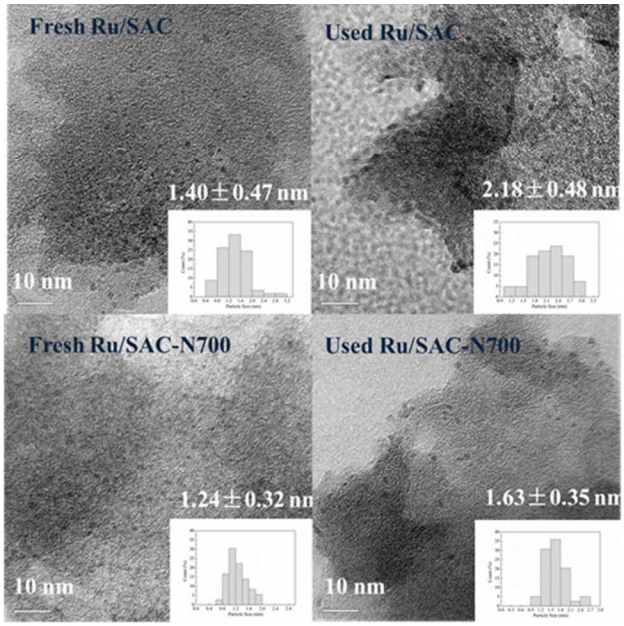

Fig. 3 TEM images of fresh and used catalysts.

The deconvolution of XPS Ru 3p3/2 spectra performed to discriminate Ru species (Fig. S4 and Fig. S5). As listed in Table 5, there are four kinds of Ru species in Ru-based catalysts, involving the metallic Ru (461.4±0.4 eV); $RuCl_3$ (463.0±0.3 eV); RuO_2 (464.5±0.4 eV) and RuO_x (465.7-467.2 eV).[40-42] The contents of Ru species are associated with the kind of support. For the fresh Ru/SAC, the dominant is $RuCl_3$ (63.0%), followed by RuOx (16.5%)> RuO_2 (13.9%)> metallic Ru (6.6%). Whereas for the Ru catalysts with the N-doped supports, the content of RuO_2 is much higher than that of Ru/SAC, but the content of $RuCl_3$ is much lower than that of Ru/SAC. In particular, the fresh Ru/SAC-N700 shows the highest content of RuO_2 (53.0%) but the lowest of $RuCl_3$ (15.4%). After experiencing 30 h of reaction, the content of RuO_2 and RuO_x decrease to some extent and the content of metallic Ru increased. It is worthwhile to note that the RuO_2 species in the used Ru/SAC-N700 is still the highest.

Table 5 The relative contents and binding energies of ruthenium species in the fresh and used catalysts

Samples	Area%, binding energy (eV)			
	Ru	$RuCl_3$	RuO_2	RuO_x
fresh Ru/SAC	6.6 (461.8)	63.0 (463.2)	13.9 (464.8)	16.5 (466.1)
fresh Ru/SAC-N600	10.1 (461.3)	47.1 (463.0)	28.5 (464.4)	14.3 (465.9)
fresh Ru/SAC-N700	20.6 (461.4)	15.4 (463.0)	53.0 (464.6)	11.0 (466.8)
fresh Ru/SAC-N800	13.0 (461.1)	25.3 (462.9)	29.4 (464.0)	32.3 (466.8)
used Ru/SAC	15.9 (461.7)	57.2 (463.4)	11.5 (464.8)	15.4 (466.1)
used Ru/SAC-N600	21.2 (461.6)	50.3 (463.5)	18.0 (464.3)	10.5 (466.3)
used Ru/SAC-N700	28.6 (461.6)	23.0 (463.1)	39.3 (414.5)	9.1 (466.7)
used Ru/SAC-N800	14.2 (461.4)	29.6 (463.2)	27.8 (464.9)	28.4 (466.3)

Moreover, Raman spectra were measured to confirm the existence of RuO_2. As shown in Fig. 4, for the Ru catalysts with the N-doped supports, there are two sharp bands at 504 and 618 cm^{-1} corresponding to the species of RuO_2,[43] and the band intensity increases in the order of Ru/SAC-N600<Ru/SAC-N800< Ru/SAC-N700. In contrast, for the catalyst Ru/SAC, the bands due to RuO_2 are relative small. It is illustrated that the N-doped supports can greatly increase the amount of the component RuO_2 in Ru catalysts, in accord with the results in Table 5.

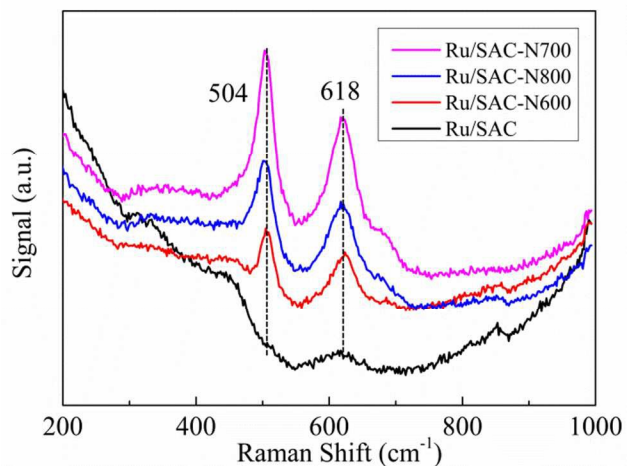

Fig. 4 Raman spectra of the fresh catalysts

According to our previous work, the pyridinic N-doped graphene support is beneficial to enhance electron transfers between the support and the active gold species

so as to stabilize the active species of Au_2Cl_6, and then increase the long-term stability of Au-based catalysts in acetylene hydrochlorination.[44] Additionally, the DFT calculations indicated that the species $RuCl_3$ could not activate efficiently the reactants of acetylene and hydrogen chloride.[45] In combination with the activity of Ru catalysts (Fig. 2), the variation of Ru species on N-doped supports (Table 5) and the contents of N species in the supports (Table 3), it is reasonable to conclude that the pyridine-nitrogen (N_P) plays an important role in augment of the catalytic activity of Ru-supported catalysts.

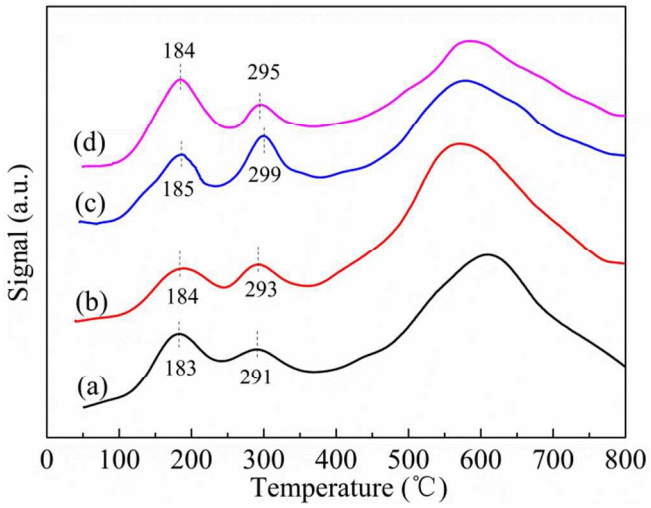

Fig. 5 H_2 TPR profiles of fresh catalysts: (a) Ru/SAC, (b) Ru/SAC-N600, (c) Ru/SAC-N700, (d) Ru/SAC-N800

Fig. 5 displays the TPR profiles of the fresh Ru-based catalysts. The broad peak in the range of 400-700 °C is attributed to the reduction of functional groups on the support. For the fresh Ru/SAC catalyst, it exhibits the peak at 183 °C together with a shoulder at 291 °C, which is attributed to the reduction of $RuCl_3$ and RuO_2, respectively.[13, 14, 17, 46] For the Ru/SAC-N catalysts, the two peaks shift to higher temperature and the peak intensity around 295 °C becomes stronger, with the maximum peak intensity corresponding to Ru/SAC-N700. The results suggesting that the N-dopants strengthen the

interaction between the supports and RuO_2 and $RuCl_3$ species.

TPD is an effective technique to study the effects of N-dopants on the adsorption properties of reactants and the product on the Ru-based catalysts. Fig. 6 displays the C_2H_2, HCl and C_2H_3Cl TPD profiles of the Ru/SAC and Ru/SAC-N700. The peak area indicates the adsorption capacity and the desorption temperature reflects the adsorption strength. As shown in Fig. 6a, the HCl desorption temperature is 150 °C on Ru/SAC, 159 °C on Ru/SAC-N700, and the adsorption capacity of HCl on Ru/SAC-N700 is much larger than that on Ru/SAC. For another reactant C_2H_2, the catalyst Ru/SAC-N700 also shows larger adsorption capacity, comparing with Ru/SAC (Fig. 6b). The trend of TPD profile for the product C_2H_3Cl is opposite with that of C_2H_2 and HCl, i.e., the adsorption capacity for C_2H_3Cl on Ru/SAC-N700 is smaller than that on Ru/SAC (Fig. 6c). Therefore, N-dopants can enhance the adsorption of reactants and the desorption of the product, consequently results in higher catalytic activity of Ru/SAC-N700.

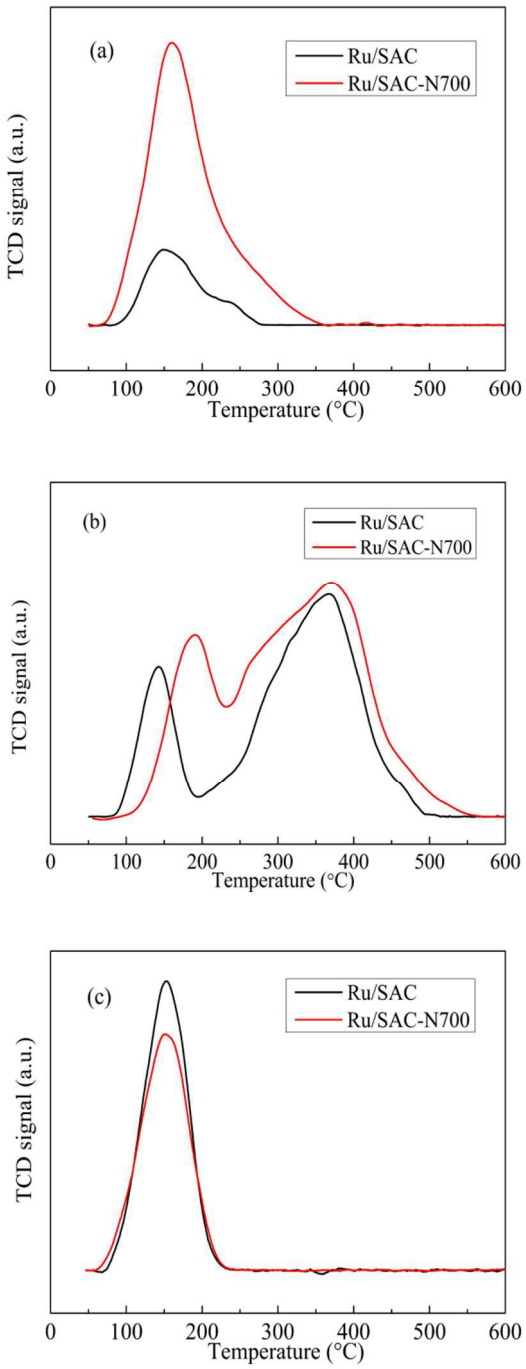

Fig. 6 TPD profiles of the catalysts: (a) HCl-TPD, (b) C_2H_2-TPD, (c) C_2H_3Cl-TPD

Further, TG was used to evaluate the degree of coke deposition on the surface of Ru-based catalysts. As shown in Fig. S6, both fresh and used catalysts have a slight weight loss before 100 °C, owing to water desorption. In the range of 100-400 °C，the

used catalysts exhibit an obvious weight loss (5.0%). When the temperature exceeds 400 °C, the fresh and used catalysts rapidly decrease in weight because the combustion of activated carbon. Taking into account the carbon support can lose its weight by reacting with oxygen in air to produce CO_2, the coke deposition is calculated by the difference of weight loss of the fresh and used catalyst in the temperature range of 100-400 °C.[47-49] Based on this method, the coke deposition of the catalysts is calculated and listed in Table 6.

As listed in Table 6, the Ru/SAC-N700 catalyst has the least coke deposition of 2.6%. The amount of coke deposition increases in the order: Ru/SAC-N700 (2.6%)< Ru/SAC-N800 (3.3%) < Ru/SAC-N600 (3.6%) < Ru/SAC (4.3%). This result is consistent with the order of catalytic activity of Ru-supported catalysts. Combining with the TPD profiles (Fig. 6), it is suggested that the larger adsorption capacities of HCl and C_2H_2, as well as the easier desorption of C_2H_3Cl result in the significant reduction of coke deposition on Ru catalysts with the N-doped support.

Table 6 Coke deposition of the catalysts

Samples	Amount of coke deposition (%)
Ru/SAC	4.3
Ru/SAC-N600	3.6
Ru/SAC-N700	2.6
Ru/SAC-N800	3.3

4. Conclusion

Ru-based catalysts with the support of N-doped spherical active carbon were prepared and assessed for acetylene hydrochlorination. The optimal catalyst Ru/SAC-N700 shows the acetylene conversion of 99.8% at the conditions of 170 °C,

C_2H_2 GHSV 180 h^{-1} and V(HCl):V(C_2H_2)=1.1:1. It is indicated that the pyridine-nitrogen plays an important role in augment of the catalytic activity of Ru-based catalysts. N-dopants can greatly increase the amount of the component RuO_2 in Ru catalysts, enhance the adsorption of reactants and the desorption of the product, and reduce significantly the coke deposition, consequently resulting in higher catalytic activity of Ru/SAC-N700. These results provide a potential route to explore high efficient Ru-based catalysts for acetylene hydrochlorination.

Acknowledgments

This work was supported by the Special Funds for the Major State Research Program of China (No. 2012CB720302), the NSFC (21176174).

References

1. J. Zhang, N. Liu, W. Li and B. Dai, *Front. Chem. Sci. Eng.* , 2011, **5**, 514-520.
2. T. K. Mackey, J. T. Contreras and B. A. Liang, *Sci. Total. Environ.*, 2014, **472**, 125-129.
3. X. Li, M. Zhu and B. Dai, *Appl. Catal. B: Environ.*, 2013, **142-143**, 234-240.
4. B. Wang, L. Yu, J. Zhang, Y. Pu, H. Zhang and W. Li, *RSC Adv.*, 2014, **4**, 15877-15885.
5. H. Zhang, B. Dai, X. Wang, W. Li, Y. Han, J. Gu and J. Zhang, *Green Chem.*, 2013, **15**, 829-836.
6. H. Zhang, W. Li, X. Li, W. Zhao, J. Gu, X. Qi, Y. Dong, B. Dai and J. Zhang, *Catal. Sci. Technol.*, 2015, **5**, 1870-1877.
7. J. Zhao, J. Xu, J. Xu, J. Ni, T. Zhang, X. Xu and X. Li, *ChemPlusChem*, 2015, **80**, 196-201.
8. K. Zhou, W. Wang, Z. Zhao, G. Luo, J. Miller, M. Wong and F. Wei, *ACS Catal.*, 2014, **4**, 3112-3116.
9. Q. Song, S. Wang, B. Shen and J. Zhao, *Pet. Sci. Technol.*, 2010, **28**, 1825-1833.
10. S. Mitchenko, E. Khomutov, A. Shubin and Y. Shul'ga, *J. Mol. Catal. A: Chem.*, 2004, **212**, 345-352.
11. S. Mitchenko, T. Krasnyakova, R. Mitchenko and A. Korduban, *J. Mol. Catal. A: Chem.*, 2007, **275**, 101-108.
12. G. J. Hutchings, *J. Catal.*, 1985, **96**, 292-295.
13. Y. Jin, G. Li, J. Zhang, Y. Pu and W. Li, *RSC Adv.*, 2015, **5**, 37774–37779.
14. G. Li, W. Li, H. Zhang, Y. Pu, M. Sun and J. Zhang, *RSC Adv.*, 2015, **5**, 9002–9008.
15. Y. Pu, J. Zhang, L. Yu, Y. Jin and W. Li, *Appl. Catal. A: Gen*., 2014, **488**, 28-36.
16. J. Xu, J. Zhao, T. Zhang, X. Di, S.Gu, J. Ni and X. Li, *RSC Adv.*, 2015, **5**, 38159-38163.
17. J. Zhang, W. Sheng, C. Guo and W. Li, *RSC Adv.*, 2013, **3**, 21062-21068.
18. M. Zhu, L. Kang, Y. Su, S. Zhang and B. Dai, *Can. J. Chem.*, 2013, **91**, 120-125.
19. L. Zhao, L. Fan, M. Zhou, H. Guan, S. Qiao, M. Antonietti and M. Titirici, *Adv. Mater.*, 2010, **22**, 5202-5206.
20. J. Liang, Y. Jiao, M. Jaroniec and S. Z. Qiao, *Angew. Chem. Int. Ed.*, 2012, **51**, 11496-11500.
21. Z. Wu, M. Benchafia, Z. Iqbal and X. Wang, *Angew. Chem. Int. Ed.*, 2014, **53**, 1-6.
22. J. Zhang, N. Nie, Y. Liu, J. Wang, F. Yu, J. Gu and W. Li, *ACS Appl. Mater. Interfaces.*, 2015, **7**, 20134-20143.
23. J. Zhang, J. Wang, Y. Liu, N. Nie, J. Gu, F. Yu and W. Li, *J. Mater. Chem. A.*, 2015, **3**, 2043-2049.

24. X. Li, X. Pan, L. Yu, P. Ren, X. Wu, L. Sun, F. Jiao and X. Bao, *Nat. Commun.*, 2014, **5**, 3688.
25. B. Dai, K. Chen, Y. Wang, L. Kang and M. Zhu, *ACS Catal.*, 2015, **5**, 2541-2547.
26. K. Zhou, J. Si, J. Jia, J. Huang, J. Zhou, G. Luo and F. Wei, *RSC Adv.*, 2014, **4**, 7766-7769.
27. W. Zhao, W. Li and J. Zhang, *Catal. Sci. Technol.*, 2015, DOI: 10.1039/C5CY01277E
28. X. Wang, J. Lee, Q. Zhu, J. Liu, Y. Wang and S. Dai, *Chem. Mater.*, 2010, **22**, 2178-2180.
29. C. Devallencourt, J. Saiter, A. Fafet and E. Ubrich, *Thermochim. Acta.*, 1995, **259**, 143-151.
30. M. S. Shafeeyan, W. M. A. W. Daud, A. Houshmand and A. Shamiri, *J. Anal. Appl. Pyrol.*, 2010, **89**, 143-151.
31. S. Biniak, G. Szymanski, J. Siedlewski and A. Swiatkowski, *Carbon.*, 1997, **35**, 1799-1810.
32. B. Yuan, M. Cao, H. Sun, T. Wang, X. Bu, D. Shi, Y. Kong and P. Li, *J. Appl. Polym. Sci.*, 2014, **11**, 40338.
33. C. Mangun, K. Benak, J. Economy and K. Foster, *Carbon.*, 2001, **39**, 1809-1820.
34. J. Przepiórski, M. Skrodzewicz and A. W. Morawski, *Appl. Surf. Sci.*, 2004, **225**, 235-242.
35. S. Bilal and R. Holze, *J. Electroanal. Chem.*, 2006, **592**, 1-13.
36. D. Mitoraj and H. Kisch, *Chem. Eur. J.*, 2010, **16**, 261-269.
37. B. Sun, W. Li and P. Wu, *Polymer.*, 2008, **49**, 2704-2708.
38. Z. Lin, M. Song, Y. Ding, Y. Liu, M. Liu and C. Wong, *Phys. Chem. Chem. Phys.*, 2012, **14**, 3381-3387.
39. Z. Sheng, L. Shao, J. Chen, W. Bao, F. Wang and X. Xia, *ACS nano.*, 2011, **5**, 4350-4358.
40. J. L. Gómez de la Fuente, M. V. Martínez-Huerta, S. Rojas, P. Hernández-Fernández, P. Terreros, J. L. G. Fierro and M. A. Peña, *Appl. Catal. B:Environ.*, 2009, **88**, 505-514.
41. J. Ma, Y. Feng, J. Yu, D. Zhao, A. Wang and B. Xu, *J. Catal.*, 2010, **275**, 34-44.
42. S. Sharma, Z. Hu, P. Zhang, E. W. McFarland and H. Metiu, *J. Catal.*, 2011, **278**, 297-309.
43. S. Mar, C. Chen, Y. Huang and K. Tiong, *Appl. Surf. Sci.*, **90,** 1995, 497-504.
44. J. Gu, Q. Du, Y. Han, Z. He, W. Li and J. Zhang, *Phys. Chem. Chem. Phys.*, 2014, **16**, 25498-25507.
45. Y. Han, M. Sun, W. Li and J. Zhang, *Phys. Chem. Chem. Phys.*, 2015, **17**, 7720-7730.
46. N. Xu, M. Zhu, J. Zhang, H. Zhang and B. Da, *RSC Adv.*, 2015, **5**, 86172-86178.
47. J. Brennan, T. Bandosz, K. Thomson and K. Gubbins, *Colloid. Surf. A:Physicochem. Eng. Asp.*, 2001, **187**, 539-568.
48. K. Dumbuya, G. Cabailh, R. Lazzari, J. Jupille, L. Ringel, M. Pistor, O. Lytken, H. P. Steinrück and J. M. Gottfried, *Catal. Today.*, 2012, **181**, 20-25.
49. D. He, X. Jiao, P. Jiang, J. Wang and Q. Xu, *Green Chem.*, 2012, **14**, 111-116.